This is to certify that the
thesis entitled

LOW BETA SUPERCONDUCTING RF CAVITY POWER COUPLER DEVELOPMENT FOR THE RARE ISOTOPE ACCELERATOR

presented by

Adam Daniel Moblo

has been accepted towards fulfillment
of the requirements for the

| Master of Science | degree in | Electrical and Computer Engineering |
|---|---|---|

Major Professor's Signature

14 Dec 2004

Date

# LOW BETA SUPERCONDUCTING RF CAVITY POWER COUPLER DEVELOPMENT FOR THE RARE ISOTOPE ACCELERATOR

By

Adam Daniel Moblo

A THESIS

Submitted to
Michigan State University
in partial fulfillment of the requirements
for the degree of

MASTER OF SCIENCE

Department of Electrical and Computer Engineering

2004

## ABSTRACT

LOW BETA SUPERCONDUCTING RF CAVITY POWER COUPLER DEVELOPMENT FOR THE RARE ISOTOPE ACCELERATOR

By

Adam Daniel Moblo

The larger more powerful accelerator facilities of tomorrow are a good match for high gradient superconducting radio frequency (rf) accelerating cavities. Coupling rf power into a superconducting rf accelerating cavity is done through a fundamental power coupler (FPC) which consists either of a waveguide or coaxial transmission line and a window to isolate the cavity vacuum. A low cost FPC design solution has been sought for the $\beta = v/c = 0.085$ 80.5 MHz quarter-wave, and the $\beta = 0.285$ 322 MHz half-wave cavities being prototyped for the Rare Isotope Accelerator (RIA). The $\beta$ of a cavity is the velocity at which a particle receives its optimum energy gain from the cavity and is expressed relative to the speed of light. The use of a commercially available vacuum rf window is the basis for the low cost design. Thermal and electrical conductivities of coupler materials are analyzed and the ohmic losses are accounted. An experimental approach is used to determine the coupler penetration lengths needed to satisfy the beam power and cavity bandwidth requirements. Two prototype FPC's and a standing wave test setup have been constructed to verify assembly procedures, power transmission, power capabilities and conditioning methods.

## ACKNOWLEDGEMENTS

These accomplishments could not have made without the help and support of my family, friends, and colleagues. Foremost I would like to thank my father and mother, Daniel and Suzanne, for the wonderful home they provided, their never-ending loving support. Also my brother, sisters and their families for always expecting more out of their younger brother. I deeply appreciate the love and support from the Ackerson family has also provided me with.

Everyone in the NSCL community has provided a friendly and enjoyable atmosphere for learning and working. The teamwork and support of the SRF accelerator group was the backbone of my research. I would like to specially thank Roger Zink for getting my foot in the door at the NSCL and Dr. Terry Grimm for the graduate educational opportunity he provided me with. I could have never done without the friendships and assistance of John Popielarski, Dr. Walter H. Hartung, Dr. John Vincent, Matt Johnson, Chris Compton, James Colthorp, Steve Bricker and John Bierwagen.

The department of Electrical and Computer Engineering has provided me with the tools and knowledge needed to become a top contributing engineer in the field of electrical engineering. I thank my advisor Prof. Leo Kempel for his dedication to my education. I also thank all the professors in the department for the wisdom they passed on to me. Finally, I thank the National Science Foundation and the U.S. Department of Energy for funding my graduate education and research.

## TABLE OF CONTENTS

## LIST OF TABLES

## LIST OF FIGURES

(Images in this thesis are presented in color.)

## LIST OF FIGURES CONTINUED

# INTRODUCTION

The quest for high gradient accelerating cavities has sparked the demand for affordable superconducting rf structures. A superconducting accelerator requires a more expensive initial investment per cavity in comparison to the alternative "normal conducting" copper structures but saves on the required quantity of cavities and the reduced rf generator power needed to power the cavity. In the Rare Isotope Accelerator (RIA) design, the reduced radio frequency (rf) power needed for the low beta cavities has opened up the opportunity for the use of commercially available hardware as an alternative to expensive over-powered fundamental power couplers (FPCs) currently in use.

The $\beta = v/c = 0.085$ 80.5 MHz quarter-wave, and the $\beta = 0.285$ 322 MHz half-wave cavities only require a generator power of 344 W and 1012 W, respectively [1]. Current commercial markets provide rf vacuum feedthroughs capable of more than 30 kW at lower frequencies. The FPC designs for the low beta cavities are adaptations of these feedthroughs. The methods used to compare electrical and mechanical tradeoffs of the design are presented. A thermal analysis was conducted to produce a low loss coupler. The construction of two prototype couplers provided a test bed for assembly procedures, impedance matching, power capabilities and conditioning procedures.

# CHAPTER 1

# THE RIA AND SUPERCONDUCTING RF CAVITIES

Numerous superconducting rf accelerating cavities are required for the Rare Isotope Accelerator (RIA) linear accelerator (LINAC) design. In all, six different cavity types will be used. The FPC designs in this paper are for specific quarter-wave and the half-wave cavities. Several cavity parameters are needed for the FPC design and can be represented in a RLC circuit model.

## 1.1 The Rare Isotope Accelerator Superconducting LINAC

The RIA is a proposed linear accelerator under prototype development. The RIA is a heavy ion accelerator, which will be able to accelerate uranium ions up to 400 MeV/u and lighter ions to higher energies with a final beam power of 400 kW.

The RIA superconducting driver LINAC consists of 496 superconducting cavities consisting of 332 low beta cavities ( $\beta$ <0.4) and 164 high beta cavities ( $\beta$ >0.4). The low beta cavities are divided into three types: $\beta = v/c = 0.041$ 80.5 MHz quarter-wave [2], $\beta = 0.085$ 80.5 MHz quarter-wave [3], and the $\beta = 0.285$ 322 MHz half-wave [4]. The power coupler development of the latter two cavities is discussed in detail throughout this paper. The high beta section consists of 6-cell elliptical structures operating at 805 MHz with betas of 0.49, 0.63, and 0.83 [5-6]. The different types of cavities are shown in Figure 1. The velocity at which a particle receives its optimum energy gain from a cavity is referred to as the

cavity $\beta$ expressed relative to the speed of light. So a particle traveling through the 322 MHz half-wave cavity section would receive a maximum energy gain at a velocity of $0.285c$. Several of each type of cavity will be arranged into a cryomodule. The cryomodules will then be aligned in ascending order according to the beta of the cavities they contain. A particle being accelerated by the LINAC would first pass through the quarter-wave cavities and into the half-waves and finally through the 6-cell elliptical cavities.

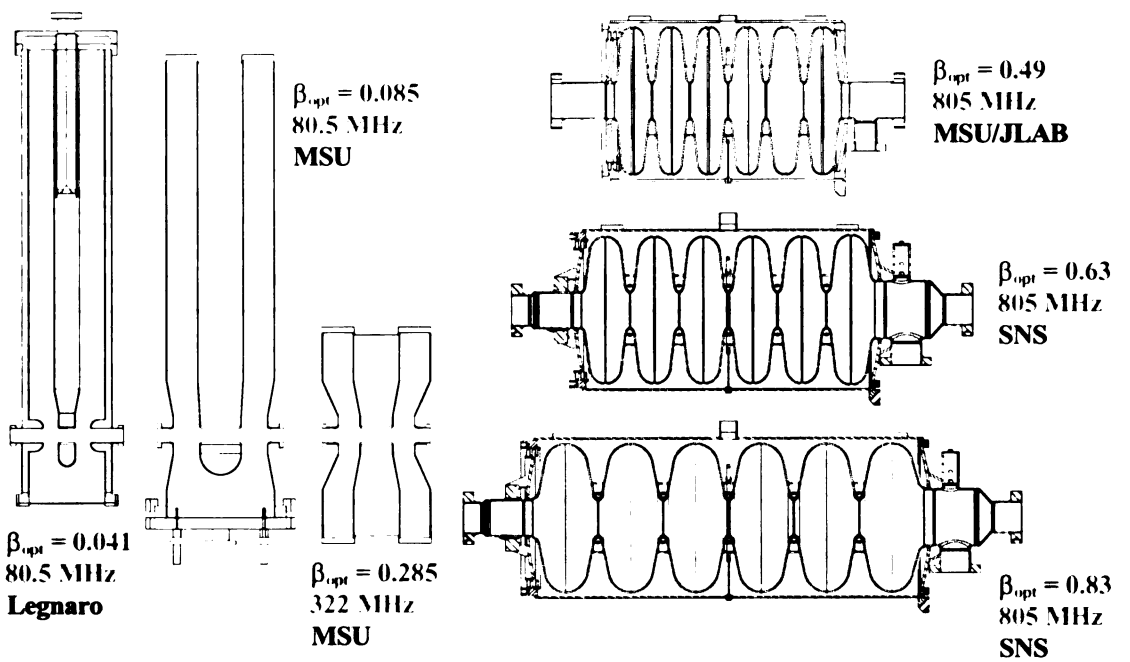


**Figure 1:** RIA superconducting LINAC cavities.

## 1.2 The Low Beta Cavities

The two low beta cavities of focus are the $\beta = 0.085$ 80.5 MHz quarter-wave, and the $\beta = 0.285$ 322 MHz half-wave. These low beta cavities are formed from RRR>150 niobium where the RRR factor is a measure of purity. The larger

the RRR, the more pure the material. Both are coaxial cavities with an outer and inner conductor diameter of 24 cm and 10, cm respectively. The cavities are indented in the beam axis region to enhance the accelerating voltage and for the quarter-wave the indentation angles are unequal to steer the beam. The quarter-wave cavities will be used for acceleration of particles in the velocity range of $v = 0.05c$ to $v = 0.15c$. The half-wave cavities will cover the $v = 0.15c$ to $v = 0.4c$ range for uranium ions and up to $v = 0.6c$ for protons. A list of operating parameters referenced throughout this paper is shown in Table 1.

| Cavity Type | | $\lambda/4$ | $\lambda/2$ |
|---|---|---|---|
| $\beta = v/c$ | | 0.085 | 0.285 |
| Frequency (MHz) | | 80.5 | 322 |
| Temperature (K) | (operating temperature) | 4.5 | 2.0 |
| $V_{acc}$ (MV) | (accelerating voltage) | 1.18 | 1.58 |
| $E_{peak}$ (MV/m) | (peak surface electric field) | 20 | 25 |
| $B_{peak}$ (mT) | (peak surface magnetic field) | 46.5 | 68.6 |
| U (J) | (stored energy) | 6.69 | 6.19 |
| $Q_0$ | (unloaded $Q$) | $5x10^8$ | $5x10^9$ |
| $Q_L$ | (loaded $Q$) | $6.3x10^6$ | $8.3x10^6$ |
| $P_{beam}$ (W) | (beam power) | 172 | 506 |
| $P_g$ (W) | (generator power) | 344 | 1012 |
| $\Delta_{allowed}$ (Hz) | (control bandwidth) | 12 | 36 |

**Table 1:** Low beta cavity parameters.

## 1.3 Cavity Parameters and the Lumped Element Model

The introduction of superconductivity introduces some parameters that may be otherwise neglected or may play a less significant role in "normal

conducting" resonators. There are several terms that have relevant importance in characterizing superconducting cavities. A simple cavity model can be used to help explain these figures of merit. A more detailed derivation can be found in [7] or [8].

Superconducting RF cavities can obtain extremely large fields ($E_{acc} > 50MV/m$ and $E_{peak} > 100MV/m$) within the cavity with relatively little input power, which explains their attractiveness as an accelerator, due to their large quality factors ($10^8$ to $10^{10}$). In the optimal case the maximum fields would be along the axis at which the particles pass through the cavity. This is not always the case so we define the accelerating field $E_{acc}$ and the corresponding voltage $V_{acc}$ as the field that the particle undergoes as it passes through the cavity, where their relationship is

$$E_{acc} = \frac{V_{acc}}{d}. \qquad 1.1$$

A superconducting RF cavity can be modeled as a resonant circuit using a simple parallel RLC circuit driven by a current source with generator impedance as shown in Figure 2. The RLC circuit can be represented as a combination of quality factors at its resonant frequency $\omega$.

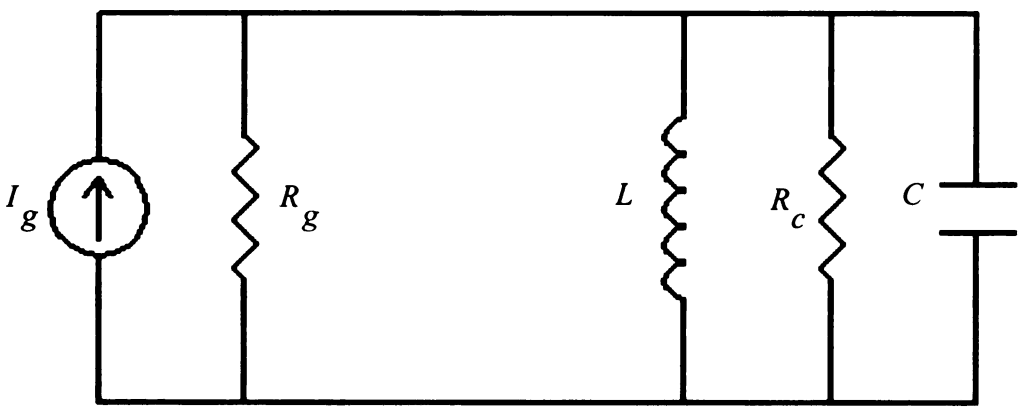


**Figure 2:** RLC model of a superconducting RF cavity.

The losses in the cavity are characterized by the unloaded quality factor $Q_0$ and is defined as:

$$Q_0 = \omega \frac{Energy\ Stored\ in\ Cavity}{Power\ Disipated\ in\ Cavity} = \frac{\omega U}{P_c} = 2\pi f R_c C\,, \qquad 1.2$$

$Q_0$ is therefore a measure of the ratio of the energy stored to the power dissipated in the cavity walls in roughly one rf cycle. The time average energy stored in the cavity corresponds to the equivalent circuit model time average energy stored in the electric field of the capacitor, which is equal to the time average energy stored in the magnetic field of the inductor. So the energy stored in the cavity can be expressed as

$$U = \frac{1}{2} C V_{acc}{}^2 = \frac{1}{2} L I^2, \tag{1.3}$$

and the power dissipated in the cavity is simply the losses across the resistor $R_c$.

$$P_c = \frac{V_{acc}{}^2}{2R_c}, \tag{1.4}$$

with $V_{acc}$ being the peak voltage of the oscillator. In terms of field quantities the time averaged stored energy is

$$U = \frac{1}{2}\mu_0 \int_v |\mathbf{H}|^2 dv = \frac{1}{2}\varepsilon_0 \int_v |\mathbf{E}|^2 dv, \tag{1.5}$$

and the dissipated power in the cavity becomes

$$P_c = \frac{1}{2} R_s \int_s |\mathbf{H}|^2 ds, \tag{1.6}$$

where $R_s$ is the surface resistance of the cavity walls, so the $Q$ of the cavity is

$$Q_0 = \frac{\omega\mu_0 \int_v |\mathbf{H}|^2 dv}{R_s \int_s |\mathbf{H}|^2 ds}. \tag{1.7}$$

Next we can define the amount of energy leaked out of the cavity and lost in the generator in terms of a quality factor. We call this the external quality factor $Q_{ext}$, which is defined as:

$$Q_{ext} = \omega \frac{Energy\ Stored\ in\ Cavity}{Power\ Disipated\ in\ the\ \text{Generator}} = \frac{\omega U}{P_g} = 2\pi f R_g C \tag{1.8}$$

We can express all the losses in the circuit, both the cavity losses and the generator losses as a quality factor also. This is called the loaded quality factor $Q_L$ and is defined as:

$$Q_L = \omega \frac{Energy\ Stored\ in\ Cavity}{Total\ Power\ Disipated\ (Cavity + Generator)} = \frac{\omega U}{P_T} = 2\pi f R_T C \qquad 1.9$$

Where $R_T$ is the parallel combination of the generator and cavity resistances.

$$R_T = \frac{R_c R_g}{(R_c + R_g)} \qquad 1.10$$

The relationship between the $Q$'s based upon their definitions is given by

$$\frac{1}{Q_L} = \frac{1}{Q_0} + \frac{1}{Q_{ext}}. \qquad 1.11$$

Next a coupling factor $\gamma_g$ can be defined between the generator and the cavity.

$$\gamma_g = \frac{Q_0}{Q_{ext}} = \frac{P_g}{P_c}. \qquad 1.12$$

Utilizing 1.12 into equation 1.11 we see that the relationship between $Q_0$ and $Q_L$ becomes

$$Q_0 = Q_L\left(1 + \gamma_g\right). \qquad 1.13$$

This equation becomes important later on in the method used to measure $Q_{ext}$.

For the case of two couplers, an input coupler and a pickup coupler, equation 1.13 becomes

$$Q_0 = Q_L\left(1+\gamma_g+\gamma_p\right). \qquad 1.14$$

Where $\gamma_g$ is the coupling factor between the generator and the cavity, and $\gamma_p$ is the coupling factor between the cavity and the pickup. Coupling factor is an appropriate name for the $\gamma$'s since they can also be written as

$$\gamma_g = \frac{P_g}{P_c}, \qquad 1.15$$

and

$$\gamma_p = \frac{P_p}{P_c}. \qquad 1.16$$

Although there are several other important parameters that are considered in the design of a superconducting cavity, the terms defined above are sufficient for designing the cavity power coupler.

# CHAPTER 2

# COUPLING POWER INTO THE CAVITY

An accelerating cavity is not complete without a FPC properly designed for the beam it's accelerating. The coupling must be set to maintain control of amplitude and phase of the beam over the cavity detuning range. The power the FPC must be able to handle can be determined from the detuning range of the cavity and the beam power. The location of the FPC on the cavity must be taken into consideration and can determine its effectiveness and adjustability. From the coupling factor we can determine the penetration length of the FPC.

## 2.1 Beam Loading and Power Requirements

The overall goal of the LINAC is to produce a beam with specified characteristics such as current and energy. The beam characteristics are what drive the cavity design and therefore the coupler design too. Once we determine the power delivered to the beam the coupler penetration length and power requirements can be determined.

The beam current is denoted as $I_b$ and the power of the beam in the cavity is defined as

$$P_b = I_b V_{acc} \cos\phi, \qquad 2.1$$

where $\phi$ is the phase with respect to the beam of the rf voltage of the cavity. In this accelerator, the phase will be -30 degrees to maintain a synchronous particle

bunch and stable longitudinal motion. Now that the power transferred to the beam is known a quality factor for the beam can be defined as was done with the cavity. The quality factor of the beam is defined as

$$Q_b = \omega \frac{Energy\ Stored\ in\ Cavity}{Power\ Disipated\ in\ the\ Beam} = \frac{\omega U}{P_b}. \qquad 2.2$$

Ideally the generator power would equal the beam power and any cavity detuning would be within the system bandwidth. For the case of RIA, cavity detuning will be greater than the system bandwidth so additional generator power is required to maintain amplitude and phase of the beam for the shift in the resonant frequency of the cavity. The required generator power $P_g$ for a given beam loading, coupler strength $Q_{ext} \cong Q_L$ and maximum detuning $\pm \delta f$ is given by [1]:

$$\frac{P_g}{P_b} = \frac{1}{4}\frac{Q_b}{Q_L}\left[\left(1+\frac{Q_L}{Q_b}\right)^2 + \left(\frac{\delta f}{\Delta_b}\frac{Q_L}{Q_b}\right)^2\right], \qquad 2.3$$

where the half beam bandwidth is

$$\Delta_b = \frac{f}{2Q_b}. \qquad 2.4$$

Assuming $P_g = 2P_b$, a system of equations can written, to determine $Q_L$ and therefore $Q_{ext}$, from equation 2.3 and by setting its derivative with respect to $Q = Q_L / Q_b$ to zero. Doing so the following is obtained

$$0 = \frac{d}{dQ}\left(\frac{P_g}{P_b}\right) = Q - \left[1 + \left(\frac{\delta f}{\Delta_b}\right)^2\right]^{-.5} . \qquad 2.5$$

By solving the system we find $Q_{ext} \cong Q_L = .33Q_b$, so the desired $Q_{ext}$ is $6.3 \times 10^6$ and $8.3 \times 10^6$ for the quarter-wave and half-wave cavities, respectively.

For $P_g = 2P_b$ the required power handling of the FPCs will be at least $4P_g$ since there is a possibility of full reflection of power from the cavity. In the case of full reflection a standing wave with twice the voltage and current of the forward wave will be formed, which equates to four times the forward power.

## 2.2 Coupler Style and Location

The focus of this paper is on the FPC development for the MSU-designed low beta cavities for the RIA. The low beta portion of the LINAC consists of half-wave and quarter-wave superconducting coaxial resonant cavities. The half-wave type is also referred to as a spoke cavity.

For the $\beta = 0.285$ 322 MHz half-wave, the fields in the cavity will be defined as follows. The z-axis is in the direction of the inner conductor axis with $z = 0$ at the beam axis and the ends of the cavity are located at $z = \pm l$ shown in Figure 3. The peak electric fields occur in the $z = 0$ plane, are radially polarized and sinusoidally goes to zero at $z = \pm l$. The peak magnetic fields occur around the $z = \pm l$ plane, are $\hat{\phi}$ polarized and go to zero at the $z = 0$ plane.

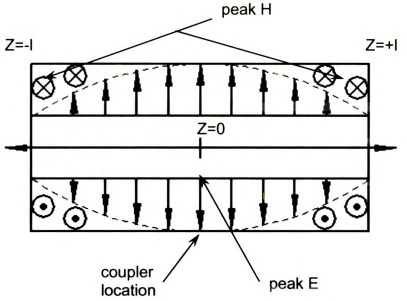


**Figure 3:** Half-wave coaxial cavity electrical and magnetic fields.

There are two practical coupler styles to choose from: a coaxial coupler with a loop to inductively couple to the magnetic field of the cavity or a coaxial coupler with a monopole antenna that capacitively couples to the electric field of the cavity. A waveguide coupler operating at 322 MHz or 80.5 MHz is impractical because of its required size. For the loop coupler the ideal location would be on the end plates of the cavity where the magnetic fields are the strongest and there are small electric fields reducing the risk of arcing. The coupling strength can then be adjusted by the size and orientation of the loop. For the capacitive coupler the ideal location would be near the $z = 0$ plane where the electric fields are the strongest and there are small magnetic fields reducing the currents on the tip of the coupler. The coupling strength can be adjusted by the length and

diameter of the monopole antenna. Capacitive coupling in the $z = 0$ plane was chosen because of its mechanical simplicity for the half-wave cavities.

For the $\beta = 0.085$ 80.5 MHz quarter-wave we will define the fields in the cavity as follows. The z-axis is in the direction of the inner conductor axis with $z = 0$ at the beam axis and the shorted end of the cavity located at $z = -l$ and the open termination at $z = +d$ shown in Figure 4. The peak electric fields occur at the open end of the cavity near the $z = 0$ plane. At $z = 0$ the electric field radially polarized and sinusoidally goes to zero at $z = -l$. For $z > 0$ the electric field is normal to the nose of the inner conductor as well as the outer conductor in this region. The peak magnetic fields occur around the $z = -l$ plane, are $\hat{\phi}$ polarized and go to zero at the $z = 0$ plane.

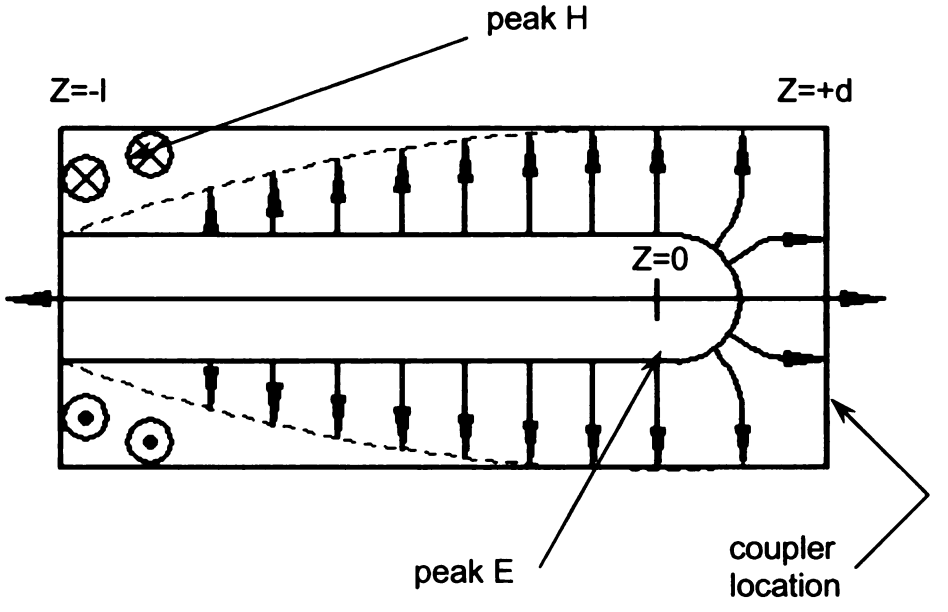


**Figure 4:** Quarter-wave coaxial cavity electrical and magnetic fields.

The practical coupler styles for the quarter-wave cavities are the same as for the half-wave explained above. The ideal location for the loop coupler is again on the short plate in the $z = -l$ plane. An appropriate location for the monopole capacitive coupler is in the $z = 0$ plane but the open end plate is a suitable choice also. The open end plate was chosen for the coupler location because of the mechanical simplicity of the design.

## 2.3 Measuring External Quality Factors

The external quality factor $Q_{ext}$ plays an important role in coupling power to the beam in the cavity since it is a determining factor in the system bandwidth. An experimental approach is used to measure the $Q_{ext}$ as a function of the coupler penetration length. A simple two-coupler method is used to measure the $Q_{ext}$ independent of the cavity losses. This means that it doesn't matter if the measurements are done when the cavity is superconducting or at room temperature.

The external quality factor $Q_{ext}$ can be calculated from the three measured parameters: the loaded quality factor $Q_L$, the reflection coefficient $S_{11}$, and the transmission coefficient $S_{21}$. All three parameters ($Q_L$, $S_{11}$, $S_{21}$) can be measured with a vector network analyzer (VNA). The two-coupler method consists of a matched input coupler ($\gamma_g \approx 1$) and a pickup coupler for

which we are interested in calculating the $Q_{ext}$. First, the definition of $Q_{ext,p}$ that is the $Q_{ext}$ of the pickup must be defined:

$$Q_{ext,p} = \omega \frac{Energy\ Stored\ in\ Cavity}{Power\ Disipated\ in\ the\ Pickup\ coupler} = \frac{\omega U}{P_p}, \tag{2.6}$$

where $P_p$ is the power of the pickup coupler which is equal to the transmitted power measured with the VNA in this setup. The $Q_{ext,p}$ can also be expressed in terms of $Q_0$

$$Q_{ext,p} = \frac{P_c}{P_p}\left(\frac{\omega U}{P_c}\right) = \frac{P_c}{P_p} Q_0, \tag{2.7}$$

where

$$Q_0 = \left(1 + \gamma_g + \gamma_p\right) Q_L. \tag{2.8}$$

$\gamma_g$ is the coupling factor between the generator and the cavity and $\gamma_p$ is the coupling factor between the cavity and the pickup. For the input coupler

$$\gamma_g = \frac{Q_0}{Q_{ext,g}} = \frac{1 \pm |S_{11}|}{1 \mp |S_{11}|}. \tag{2.9}$$

Where the sign is chosen so that $\gamma_g$ is greater than one when over-coupled and less than one when under-coupled. $Q_0$ may be approximated as

$$Q_0 \approx \left(1 + \gamma_g\right) Q_L \approx 2Q_L. \tag{2.10}$$

This approximation of $Q_0$ is most accurate when the input coupler is matched ($\gamma_g \approx 1$), since the range of $Q_{ext,p}$ is 1x10$^6$ to 1x10$^7$, then $\gamma_p << \gamma_g$ is satisfied.

The power dissipated in the cavity $P_c$ can be approximated as the forward power less the reflected power of the matched input coupler,

$$P_c = P_f - P_r. \tag{2.11}$$

Where the reflected power is ($P_r \approx 0$ for the matched input coupler) given by

$$P_r = |S_{11}|^2 P_f. \tag{2.12}$$

The power of the pickup is

$$P_p = |S_{21}|^2 P_f. \tag{2.13}$$

Substituting equations 2.11, 2.12, and 2.14 into equation 2.7 results in the calculated value of $Q_{ext,p}$ from the measured parameters of $Q_L, S_{11}$ and $S_{21}$.

$$Q_{ext,p} \approx \frac{1-|S_{11}|^2}{|S_{21}|^2}(1+\gamma_g)Q_L \approx \frac{2Q_L}{|S_{21}|^2}. \tag{2.14}$$

By means of the two-coupler method described above, the $Q_{ext}$ of the pickup coupler in the measurement is plotted as a function of antenna length in Figure 5 and Figure 6. From these plots we can determine the length of the antenna to achieve the proper coupling of the FPCs.

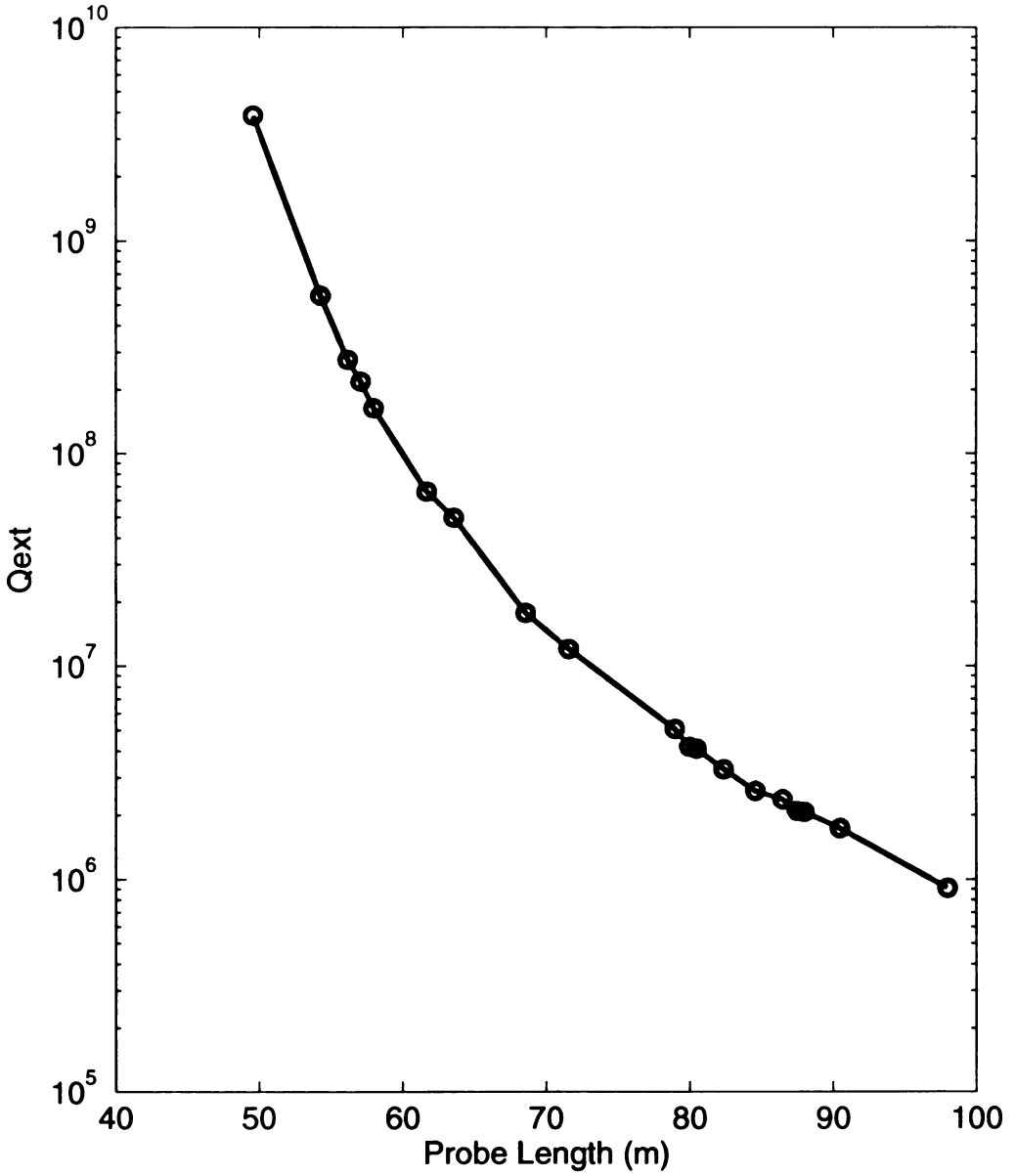


**Figure 5:** Qext vs coupler probe length for the 80.5 MHz cavity where the length is measured into the cavity from the stainless steel mini CF flange of the bottom plate of the cavity.

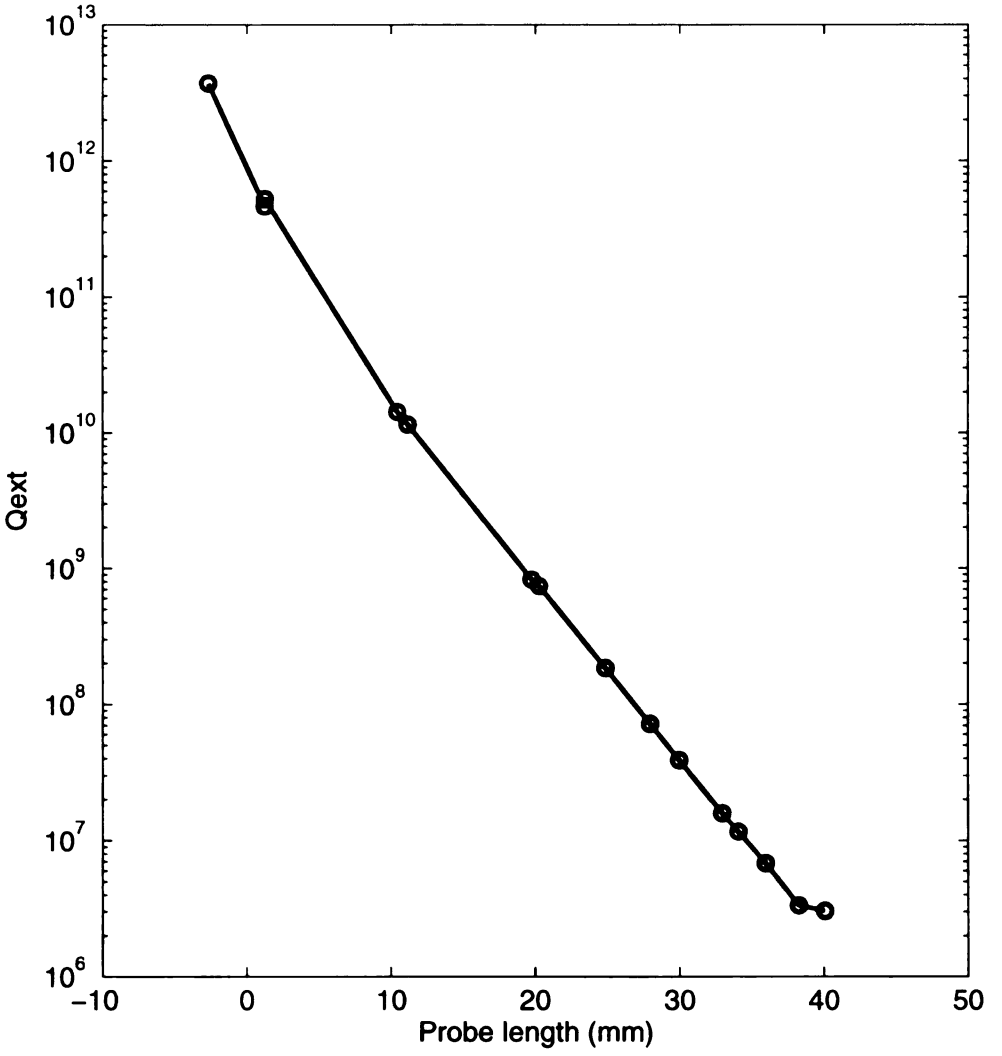


**Figure 6:** Qext vs coupler probe length for the 322 MHz cavity where the length is measured into the cavity from the surface of the NbTi CF flange of the cavity.

# CHAPTER 3

# MECHANICAL CONSRAINTS

Coupling power into a superconducting RF cavity poses several mechanical design issues. First of all the materials must be able to withstand cryogenic temperatures, withstand large pressure differentials, create an ultra-high vacuum seal with the mating cavity, and be unsusceptible to outgassing harmful contaminants into the rest of the cavity. Second, the thermal load to the cryogenics system should be minimized to maximize the cryomodule efficiency (it takes about 1 kW of electrical power to remove 1 watt of heat from 2 K liquid helium due to Carnot and mechanical efficiencies). Lastly there are constraints on the physical size of the coupler to create the correct impedance as well as reduce the effects of multipacting. A balance must be made between the mechanical constraints and the electrical performance.

## 3.1 Material Constraints

The materials of choice for ultra-high vacuum systems are 304 stainless steels, OFHC (oxygen free high conductivity) copper, aluminum and ceramics [9]. Since ceramics are not a good electrical conductor, it is a good choice as an electrical insulator of vacuum window in our case. Aluminum is subject to outgassing due to its inherent oxide layer present on its surface. Stainless steel and OFHC copper would be a good choice of materials for the power coupler. The mating flange on the cavity is a stainless steel conflat flange that can only be

sealed with another mating conflat with a copper vacuum gasket between them. The airside end of the coupler must be welded to a stainless steel bellows to allow for the shrinkage of the cavity when it cools down to less than 5 K. For these reasons investigation of the use of 304 stainless steel as a potential material for the outer conductor is necessary.

Thermal conduction properties must be investigated to minimize the conduction of heat into the helium cooling system. A simple solution to minimize the heat flow is to make the walls of the outer conductor thin, which reduces the cross sectional area for the heat to flow through. This concept is easily seen from the following heat equation known as Fourier's Law [10]

$$q_{cond} = k(T)A\frac{dT}{dx}, \qquad 3.1$$

where $q_{cond}$ is heat conduction in watts, $k(T)$ is the thermal conductivity of the material which is dependent on temperature $T$ and $A$ is the cross sectional area at which the heat passes through. If we reduce $A$ then $q_{cond}$ is reduced. For stainless steel $k(T)$ decreases as $T$ decreases, this is ideal and shown in Figure 7 along with the thermal conductivity of OFHC copper as well [11]. It can be seen that the 304L stainless steel is a better choice than OFHC copper in reducing the conduction of heat.

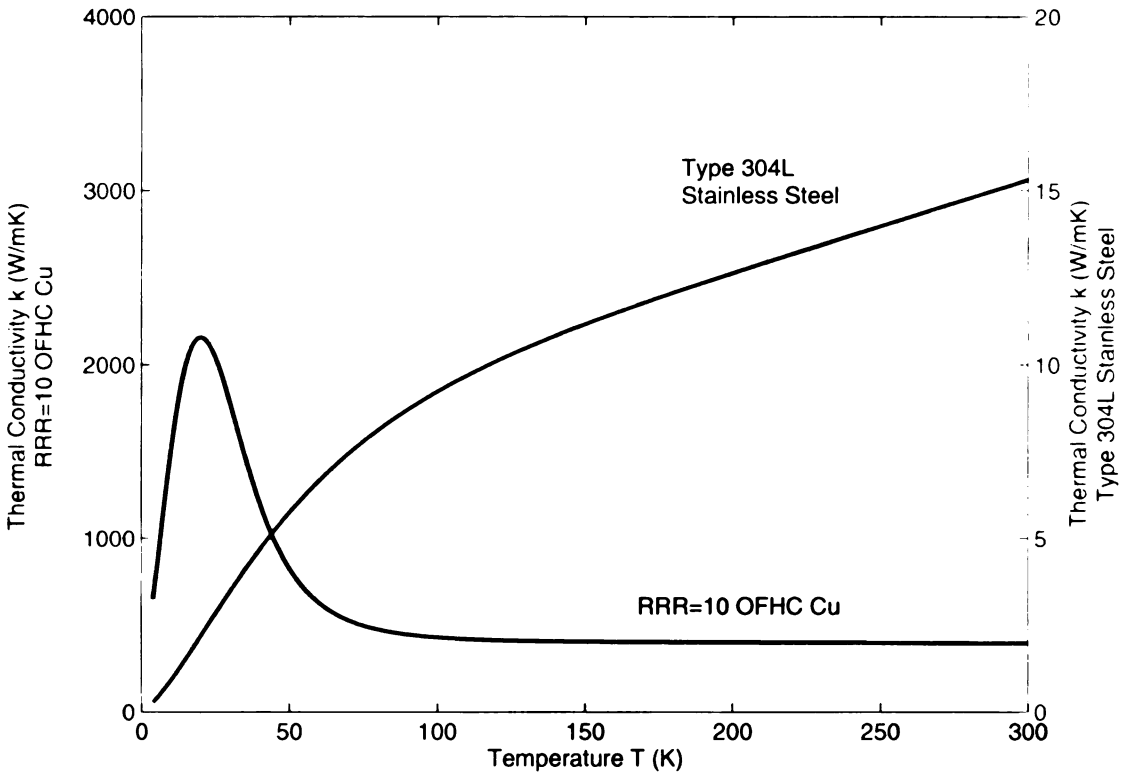


**Figure 7:** Thermal conductivity of select materials.

Another source of heat in the outer conductor is the ohmic losses in the conductor material. The electrical resistivity, shown in Figure 8 [11], is another dominating factor in the choice of material to suppress large ohmic losses in the outer conductor. Ohmic losses are characterized by [12]

$$q_{rf} = \frac{1}{2} I^2 \frac{\rho x}{2\pi r \delta}. \qquad 3.2$$

where

$$\delta = \sqrt{\frac{\rho}{\pi \mu_0 f}} \qquad 3.3$$

is the skin depth, $\rho$ is the resistivity of the material, $r$ is the radius of the outer conductor and $x$ is the length of the coupler. Hence, the ohmic losses are less

for a material with a lower resistivity. The OFHC copper is the better choice for reducing ohmic losses.

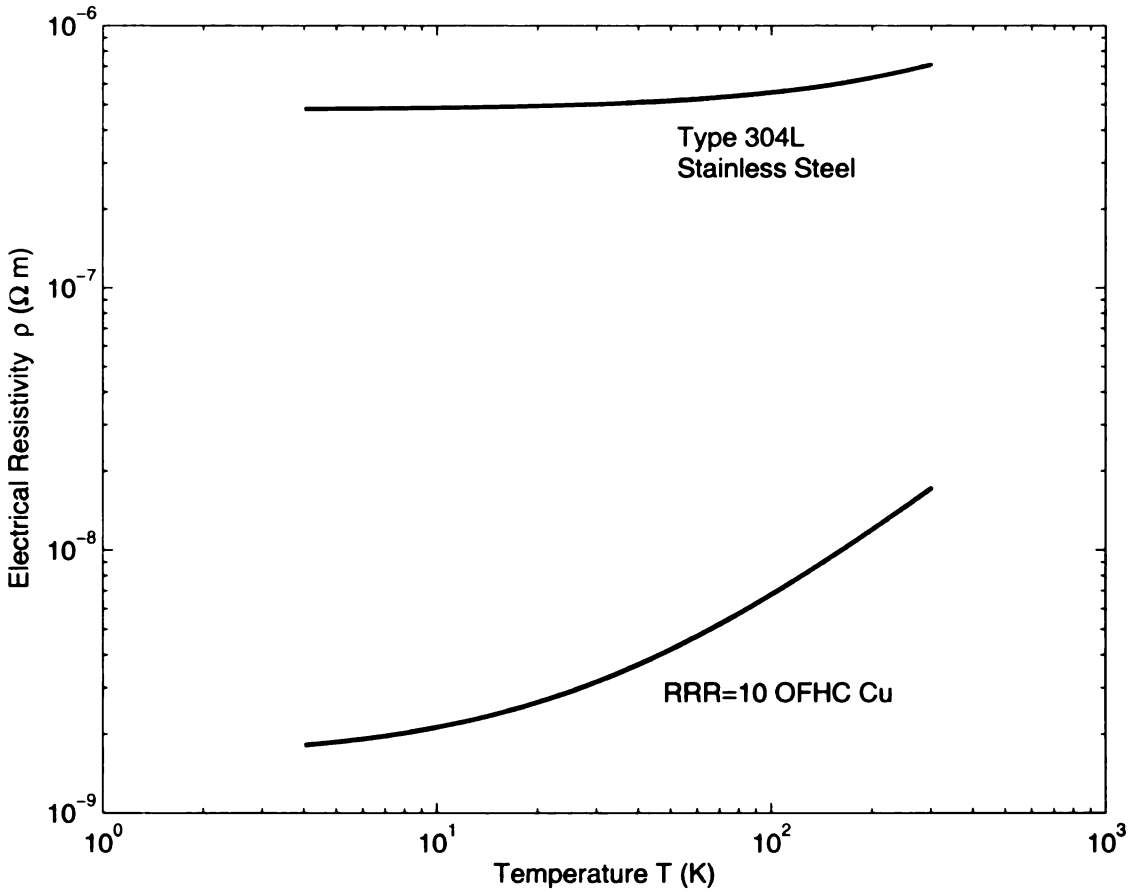


**Figure 8:** Electrical resistivity of select materials.

A decision must be made between the stainless steel and copper to construct the outer conductor. The ohmic losses in the stainless steel are unacceptable since the heat delivered to the helium system would be larger than one watt (the design maximum). The thermal conduction of the copper conducts too much heat from the 300 K end of the coupler into the 2-4.5 K helium system, again larger than one watt. Since neither material by itself will satisfy the design

criteria, a combined material solution was developed using a thin walled (.020 inch wall) 304L stainless steel tube with the inner surface plated with an $8-16\mu m$ layer of OFHC copper. The thin copper layer reduces the ohmic losses from the stainless steel as well as reduces the thermal conduction from an equivalent pure copper outer conductor. By adjusting these parameters an optimum design solution was found minimizing ohmic heating and conduction heat transfer.

The inner conductor can be made from all OFHC copper since there is no conduction path to the helium system and also the vacuum window of the coupler already has a copper inner conductor to mate to.

## 3.2 Thermal Analysis

The cavity temperature of the 322 MHz cavities is 2 K and 4.5 K for the 80.5 MHz cavities [1,3-4]. The outer conductor of the power coupler provides a direct conduction path for heat transfer between the outside of the cryomodule to the cavity, which are at 300 K and 2-4.5 K respectively. To maximize the thermal efficiency of the cryomodule, this conduction path should be minimized.

The heat dissipated into the liquid helium bath of the cavity is specified to be less than one watt per coupler. The total heat $q_{total}$ is the sum of the rf losses in the outer conductor, the power radiated by the warmer inner conductor and the conduction along the coupler axis [13].

$$q_{total} = q_{cond} + q_{rf} + q_{rad}. \qquad 3.4$$

Where equation 3.1 utilizes

$$k(T)A = k_{ss}(T)A_{ss} + k_{cu}(T)A_{cu}, \tag{3.5}$$

for the parallel conduction paths of the stainless steel and the copper plating. The radiated power $q_{rad}$ from the inner conductor is [14]

$$q_{rad} = \frac{\sigma_{SB} A_{ic}(T_{ic}^4 - T_{oc}^4)}{\frac{1}{\varepsilon_{ic}} + \left(\frac{1}{\varepsilon_{oc}} - 1\right)\frac{A_{ic}}{A_{oc}}}, \tag{3.6}$$

where $\varepsilon$ is the emissivity and $\sigma_{SB}$ is the Stefan-Boltzmann constant. The rf losses are as described in equation 3.2 where the current is assumed to be constant along the conductor and is calculated as

$$I = \sqrt{\frac{8P}{Z}}. \tag{3.7}$$

This is the maximum peak current when a standing wave is present. This approximation for the current will result in larger calculated rf losses than what will appear in reality.

A reverse difference model was constructed to calculate $q_{total}$ and the temperature profile along the outer conductor. The temperature is defined at the cavity as 2 K or 4.5 K and again at the 77 K thermal intercept. In Figure 9 and Figure 10, the total heat $q_{total}$ is plotted for a given copper plating thickness as a function of length from the cavity to the 77 K intercept. The 77 K intercept is chosen to minimize the conduction and rf loss heating.

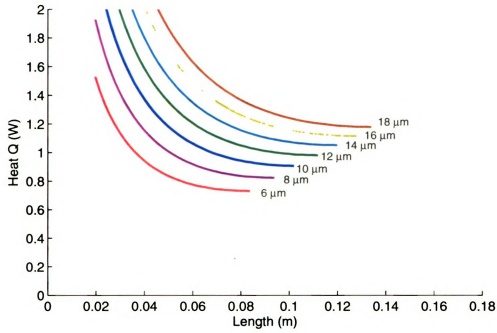


**Figure 9:** Heat dissipated in the helium system for select copper plating thicknesses due to the power coupler for the 322 MHz half-wave cavity.

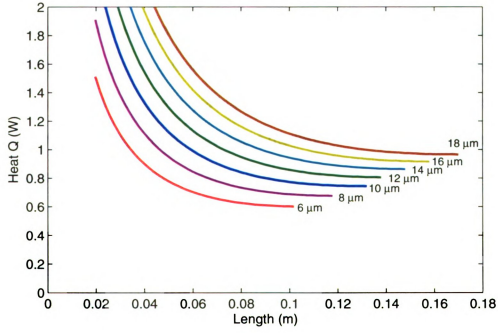


**Figure 10:** Heat dissipated in the helium system for select copper plating thicknesses due to the power coupler for the 80.5 MHz quarter-wave cavity.

## 3.3 Plating Measurements

Verifying the thickness of the copper plating on the outer conductors is a critical step in the construction of a superconducting cryomodule. If the copper plating is too thick, a static heat load would be added to the cryomodule causing added stress on the cryogenics system. If the copper plating is too thin the electric field will penetrate into the stainless steel inducing currents causing large ohmic losses in the outer conductor. This again will dramatically increase the heat load on the cryogenics system.

Measuring the thickness of the copper plating, which is on the order of 8 to 16 micrometers, can be a tricky task to handle accurately. The most accurate method would be to cut a cross section and measure the thickness under a microscope, but that is not a possibility due to its destructive nature. A second method would be to measure the mass of the conductors before plating and then again after the plating and calculate the thickness due to the difference in mass. The technique used was to apply a known DC current $I$ thought the conductor and measure the voltage drop $V$ across a measured distance $l$. From this, the total resistance of the conductor can be calculated.

$$V = I * R_{total}, \tag{3.8}$$

where $R_{total}$ is the parallel combination of $R_{ss}$ (the resistance of the stainless steel) and $R_{cu}$ (the resistance of the copper plating).

$$R_{total} = \frac{R_{ss} R_{cu}}{R_{ss} + R_{cu}} \ (\Omega). \qquad 3.9$$

After solving equation 3.9 for $R_{cu}$, the thickness of the copper plating can calculated.

$$R_{cu} = resistivity\left(\frac{length}{area}\right) = \rho_{cu}\left(\frac{l}{A_{cu}}\right) \ (\Omega). \qquad 3.10$$

$$A_{cu} = \pi r^2 - \pi(r - t_{cu})^2 \approx 2\pi r t_{cu}. \qquad 3.11$$

By solving equation 3.10 for $A_{cu}$ and substituting in equation 3.11, $t_{cu}$ (the copper plating thickness) can be determined.

$$t_{cu} = r - \sqrt{r^2 - \frac{\rho_{cu} l}{\pi R_{cu}}} \approx \frac{\rho_{cu} l}{2\pi r R_{cu}}, \qquad 3.12$$

where $r$ is the inner radius of the outer conductor, or in other words, the radius at the stainless steel / copper interface.

To minimize the error, the measurements were done at a temperature of 77 K. The conductors were submersed in liquid nitrogen during the measurements to obtain a temperature of 77 K. For the specified copper thickness of 12 micrometers, Figure 11 shows the contribution of the resistance of the copper and the resistance of the stainless steel to the total resistance, which is measured.

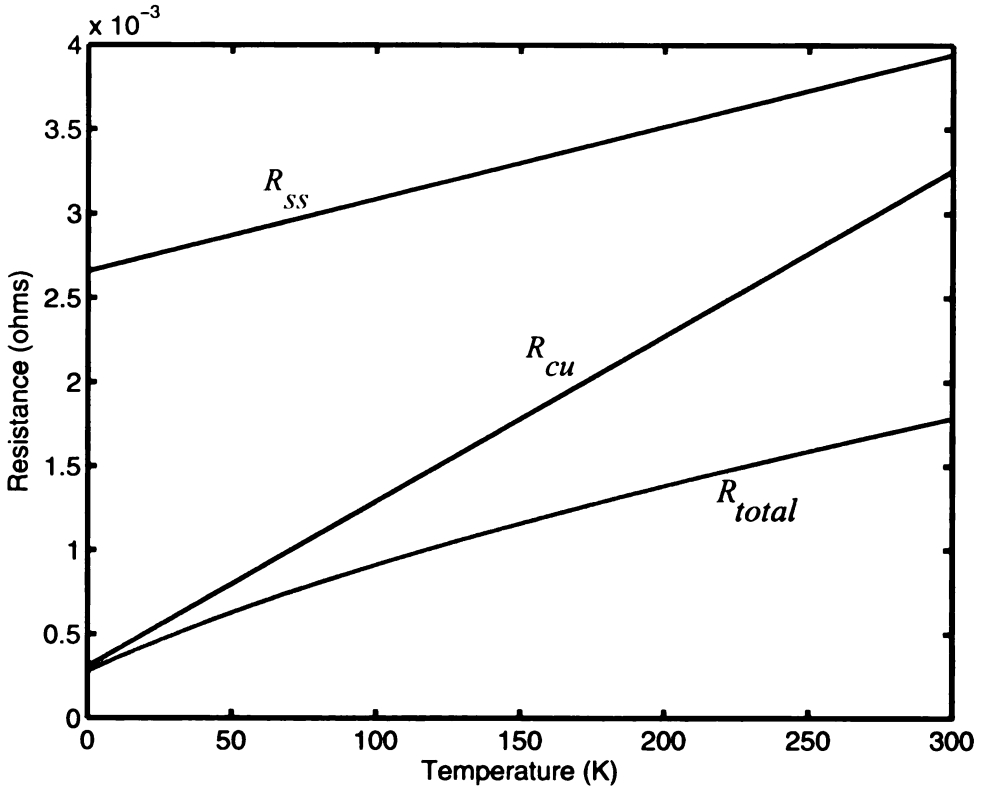


**Figure 11:** Resistance per unit length.

From Figure 11 it is easy to see that the total resistance is dominated by the copper plating resistance at 77 K. Since the measured resistance is dominated by the resistance of the copper plating, the error in knowing the stainless steel resistance has less effect on the measured plating thickness.

## 3.4 Vacuum Window, Conductor Size and Multipacting

The vacuum window of the coupler, which isolates the cavity vacuum from room air, can be an expensive item to develop from scratch. For this reason a commercial window was sought. The coupler requires the window to be non-magnetic, able to withstand bake out temperatures, low loss, well matched at the

cavity frequency and be able to handle the appropriate power. An rf feedthough from Insulator Seal was chosen for the window assembly [15].

The window is made from >94% alumina ceramic insuring low loss at 322 MHz and 80.5 MHz and a high temperature threshold. The inner conductor is made from 0.25 inch OFHC copper, and is mounted on a standard 2.75 inch diameter stainless steel conflat flange.

The diameter of the inner and outer conductors is not only critical to the thermal analysis but also determines the impedance of the coupler and can determine the power levels at which multipacting will occur. Since the vacuum window already has a 0.25 inch diameter inner conductor that will become the starting point for the design. To reduce cost and simplify the manufacturing, an attempt was made to use standard tubing sizes for the inner and outer conductor.

To determine the outer diameter of the coupler, a characteristic impedance for the coupler must be specified. The transmission line mating to the coupler will have a characteristic impedance of $50\,\Omega$, therefore making the impedance of the coupler $50\,\Omega$ would be the practical choice. Other impedances are possible but would require the addition of an impedance transformer to match the coupler to the transmission line further complicating the design. For an inner conductor diameter of 0.25 inches and a characteristic impedance of $50\,\Omega$, the outer conductor diameter can be calculated from [16]

$$Z_0 = \frac{\eta_0}{2\pi} \ln\left(\frac{d_{oc}}{d_{ic}}\right). \qquad 3.13$$

and is about 0.576 inches. Here the wave impedance of free-space is given by

$$\eta_0 = \sqrt{\frac{\mu_0}{\varepsilon_0}} \approx 377\,\Omega. \qquad 3.14$$

The inner diameter of a standard 0.625 inch diameter, .020 inch wall 304L stainless tube is 0.585 inches, which corresponds to a characteristic impedance of $51\Omega$. The reflection coefficient between the $50\Omega$ transmission line and the $51\Omega$ coupler can be calculated as

$$\Gamma = \frac{Z_{trans} - Z_{coupler}}{Z_{trans} - Z_{coupler}} = \frac{50-51}{50+51} = -.010. \qquad 3.15$$

The reflected power then becomes

$$P_r = |\Gamma|^2 P_f \cong 0. \qquad 3.16$$

So an inner conductor made from 0.25 inch diameter copper rod and a outer conductor constructed from standard 0.625 inch diameter, .020 inch wall 304L stainless tubing will satisfy the impedance criteria for the coupler.

Multipacting is another driving force behind the diameter of the coaxial coupler. Multipacting is a resonant condition that occurs in rf structures when an electron is emitted from the surface of the conductor and accelerated by the rf field. If the resonant condition is met when the electron hits the surface several more electrons may be emitted and accelerated by the rf fields. This can lead to large power losses in the conductor and cause additional heating to the coupler as well as unwanted outgassing into the cavity. For coaxial transmission lines the power levels at which multipacting can occur is proportional to the frequency

and the diameters of the inner and outer conductors. For one-point multipacting (from inner or outer conductor back to itself), the multipacting power is

$$P_{\text{one}-\text{point}} \sim (fd)^4 Z, \qquad 3.17$$

and for two-point (from inner to outer and back) this becomes

$$P_{\text{two}-\text{point}} \sim (fd)^4 Z^2. \qquad 3.18$$

From the analysis done in [17], it was estimated that the power levels at which multipacting is most likely to occur are relatively low compared to the operating power levels of the couplers. An estimate of <10 watts for the 322 MHz coupler and <1 watt for the 80.5 MHz coupler compared to their operating power levels of 1012 watts and 344 watts, respectively.

# CHAPTER 4

# PROTOTYPE ASSEMBLEY, TESTING AND CONDITIONING

The assembly of two prototype couplers has been constructed to verify their performance. The two-coupler setup must be thoroughly cleaned to prevent contamination of the accelerating cavity. The coupler will endure a bake-out process to drive out any gasses within the material. The couplers will also be tested to verify that they can meet the power capacity required of them.

## 4.1 Prototype Assembly and Cleaning

A test setup was designed to test and condition two couplers simultaneously. For the 805 MHz couplers, a waveguide was used to join the couplers together; however, that is not practical since the size of a 322 MHz and 80.5 MHz waveguides would be extremely large. The connection between the two couplers was instead made with a cylindrical copper sleeve which shorted them together as shown in Figure 12. The outer conductors were extended through the vacuum assembly needed to pump out the couplers. During high power testing the inner conductor joint limited the power capabilities. When high power was applied the rf losses on the inner conductor heated the joining sleeve causing it to expand and loosen the inner conductor union. A slotted sleeve with tighter tolerances would be a better choice for the inner conductor connector.

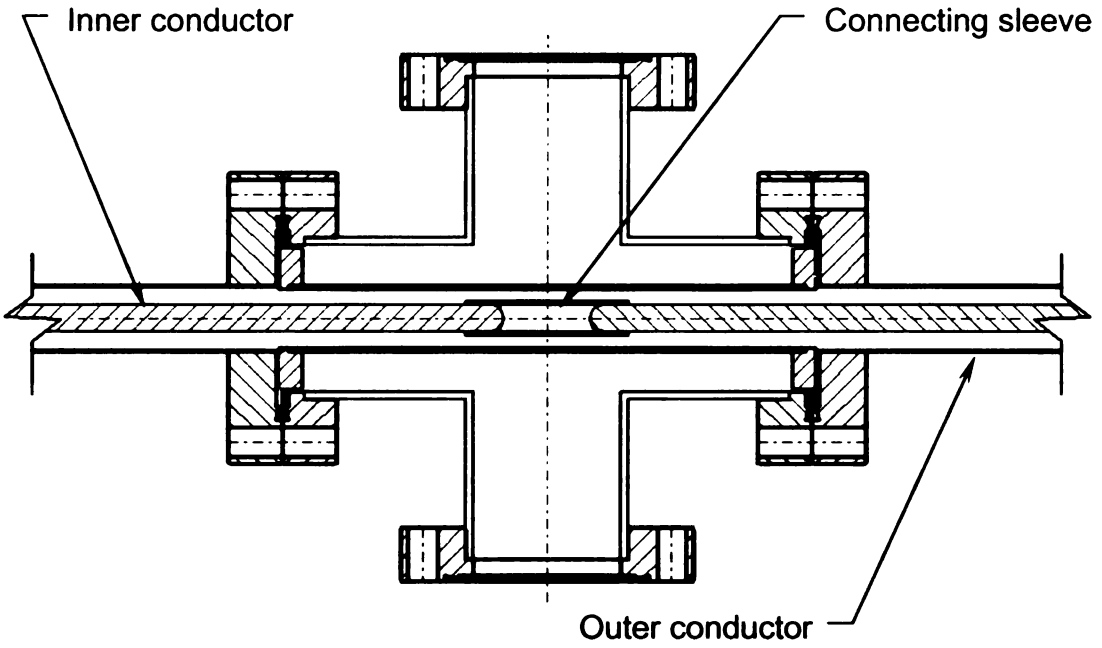


**Figure 12:** Two-coupler test setup conductor joints.

All cavity vacuum components must be assembled in a class 100 clean room to prevent particle contamination to the cavity. Any particle contamination can cause a devastating reduction in performance of the cavity due to field emission. The power couplers share the cavity vacuum and therefore require cleaning and assembly in the clean room. All coupler components exposed to the cavity vacuum including the inner conductor window assembly and the copper plated outer conductor must be cleaned with a micro-90 solution in the ultrasonic cleaner and rinsed with ultra pure water. The two-coupler test setup requires the same clean room processing and assembly.

## 4.2 Bake-out Procedure and Results

A procedure referred to as a bake-out is used to drive out absorbed gasses from the coupler walls. By heating the coupler we can expel the water remaining from the cleaning process and other gasses within the walls. Once the materials are evaporated out of the coupler walls into gaseous form the vacuum pump can remove them from the setup.

The bake-out procedure is quit simple. Thermocouples were placed on the outer and inner conductors of each coupler to monitor the temperature. A heat tape was then wrapped around the two-coupler test assembly and encased with aluminum foil to retain the applied heat. The temperature was then ramped up until all parts of the assembly reached a temperature of $>100\ ^{o}C$. The temperature was maintained until the vacuum pressure stopped showing much improvement. The temperature profiles of the bake-out are shown in Figure 13 and the vacuum pressure can be seen in Figure 14.

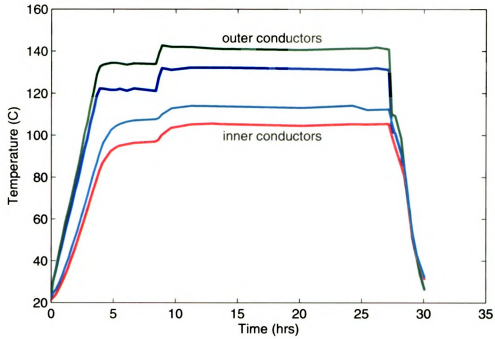


**Figure 13:** Temperature profile during the two-coupler test setup bake-out.

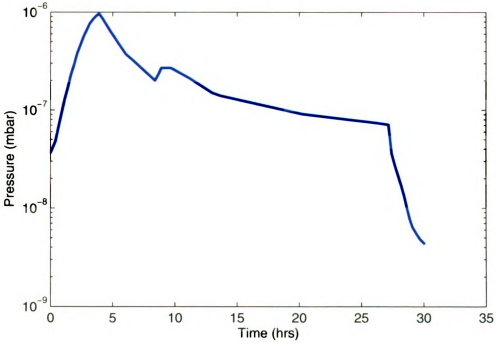


**Figure 14:** Vacuum pressure of the two-coupler test setup during bake-out.

The temperature profile in Figure 13 shows a difference between temperature sensors. This is due to there placement in the test setup. The outer conductor thermocouples were positioned between the heat tape and the outer conductor so the actual temperature of the outer conductor may be lower than the measurement. The inner conductor thermocouples were positioned inside the inner conductor where a good thermal contact could not be made therefore the inner conductor temperature was likely to be higher than the measured value. In conclusion the temperature of all the vacuum surfaces of the coupler reached a value of $>100\ ^{o}C$.

## 4.3 Matching Parameters

The reflection and transmission coefficients are two important parameters in evaluating the rf performance of the couplers. If the couplers are not properly matched a large portion of the power being sent to the cavity will be reflected back to the source. The measurements were conducted by attaching the ports of the network analyzer to the two-coupler setup via 1-5/8 EIA to type-N adapters. The reflection measurements were conducted by placing a $50\,\Omega$ load at one port and measuring the reflection coefficient from the other port. Reflection measurements were conducted from both ports and their results were identical. The transmission measurement was conducted by attaching both ports of the network analyzer to the two ports of the couplers via the 1-5/8 EIA to type-N

adapters. The measured results of the reflection and transmission coefficients are presented in Figure 15 and Figure 16, respectively.

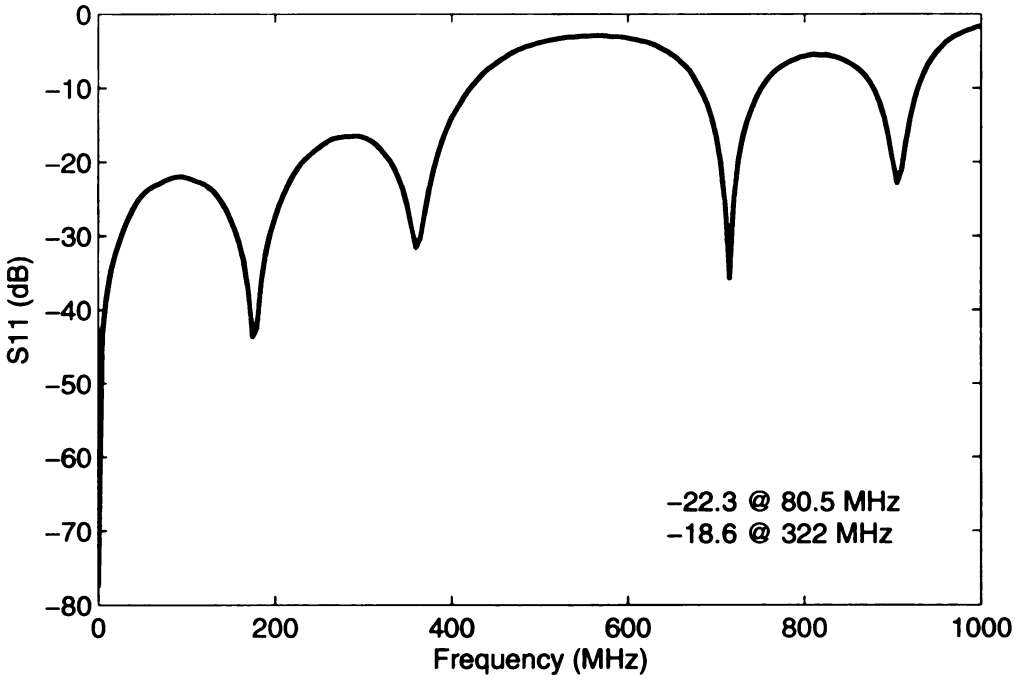


**Figure 15:** The reflection coefficent through the two-coupler test setup.

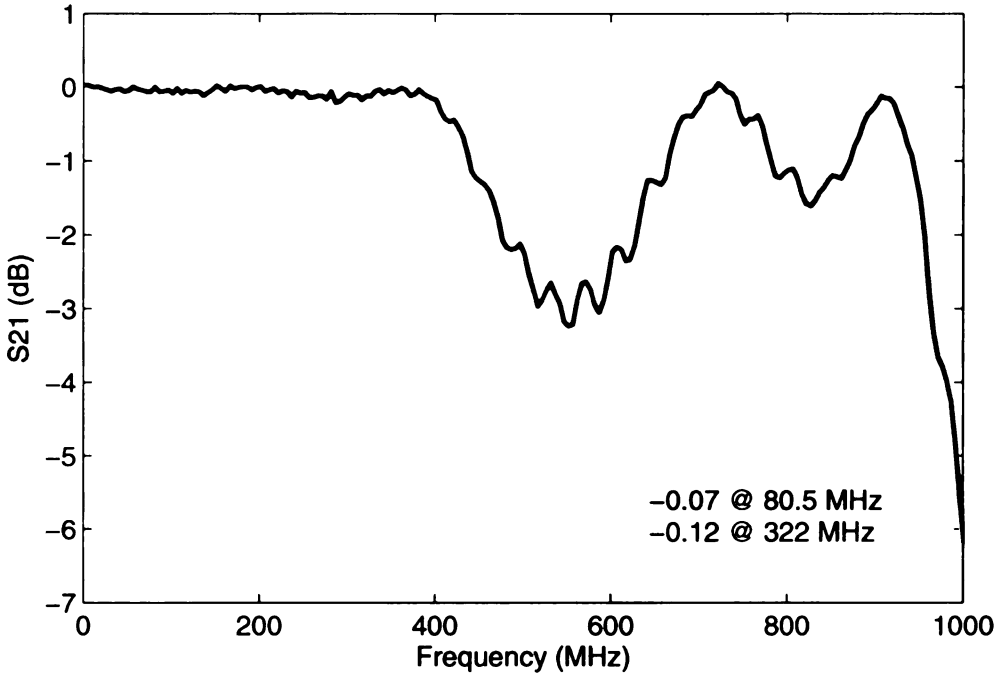


**Figure 16:** The transmission coefficent through the two-coupler test setup.

The measured results do not account for the reflections and losses within the 1-5/8 EIA-to-type-N adapters used for the measurements or the coupler to coupler union. Therefore the true reflection and transmission coefficients of the couplers are speculated to be lesser and greater, respectively. The matching between the $50\,\Omega$ transmission line and the couplers at the design frequencies are acceptable for their application.

## 4.4 Power Testing and Conditioning

The generator power currently available produces significantly less than the design power for the couplers. A standing wave cavity was constructed to overcome the lack of generator power. With the use of a resonant cavity, the

equivalent voltages and currents that the coupler would endure at the full power levels can be achieved.

The resonator cavity is a coaxial cavity partially constructed from the two-coupler test setup to expose the couplers to the standing wave fields of the cavity. One end of the cavity is an open coaxial termination at which rf power can be easily capacitively coupled. The other end of the cavity is a coaxial sliding short that can easily adjust the length of the cavity and therefore the frequency and standing wave pattern as well. The setup is shown in Figure 17.

The goal of the high power test is to expose the coupler to larger voltages and currents than the design will require during operation. The most vulnerable part of the coupler to fail is arching at the vacuum window. The electric field of the coupler is shown in Figure 18. To accomplish this, the standing wave pattern can be adjusted to maximize the current or the voltage at the vacuum window location. The standing wave patterns for the voltage and current are assumed to be sinusoidal since the length of the resonator is dominated by free space, only a small fraction of the length is alumina. For the open termination at the input coupling end the boundary conditions are that the voltage will be maximum and the current zero. At the sliding short end of the cavity the current will be maximum and the voltage zero.

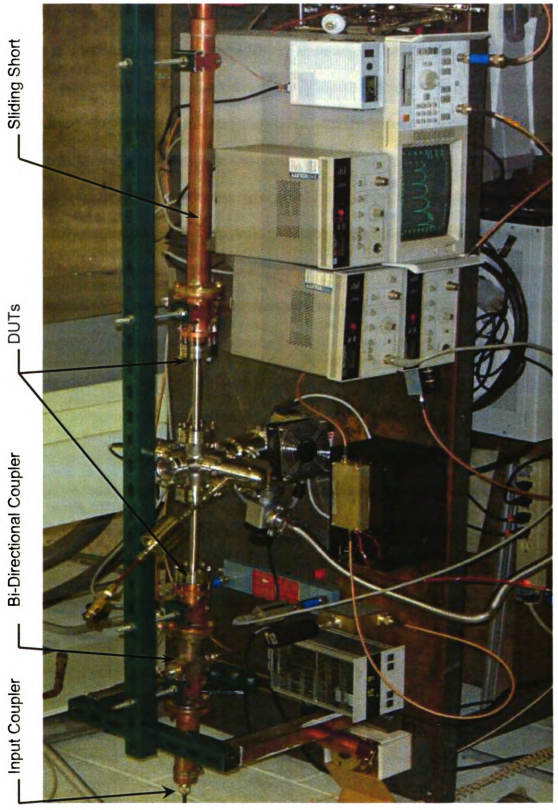


**Figure 17:** Two-coupler test setup for high power testing and conditioning.

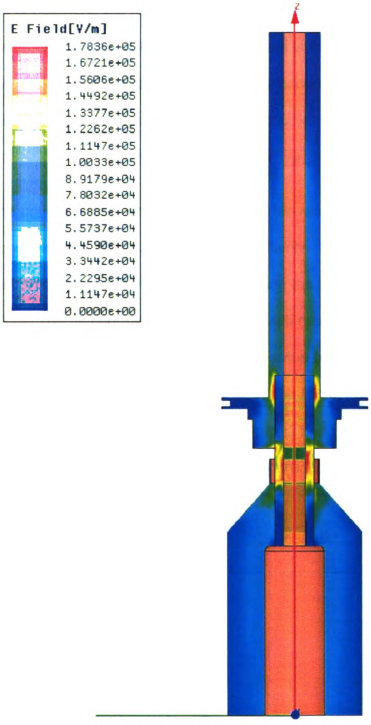


**Figure 18:** Electric field simulation for the coupler at 322 MHz with 1 kW applied to the 1-5/8" EIA input of the coupler and the cavity port shorted to produce the equivalent maximum standing wave fields the coupler will endure during operation using Ansoft's HFSS software package.

The peak voltage of the FPCs can be estimated from the impedance of the coupler and the required power. The peak voltage that could occur will be the standing wave voltage when the beam is not present and the coupler is no longer matched to the cavity. When this occurs all the power is reflected from the cavity and the peak voltage on the coupler becomes

$$V_p = 2\sqrt{P_{avg} 2R}\,. \qquad 4.1$$

The corresponding voltages for the quarter-wave and half-wave FPCs are approximately 370 V and 640 V, respectively. In the test setup the peak voltage can be calculated the same way but using the line power instead.

The two-coupler test setup is a multi resonant cavity. There are an infinite number of resonant frequencies for the setup but only the first few have relevance since they are in the range of the FPCs frequencies. The first four resonant frequencies are shown in Figure 21 and their corresponding voltage standing wave patterns are shown in Figure 22.

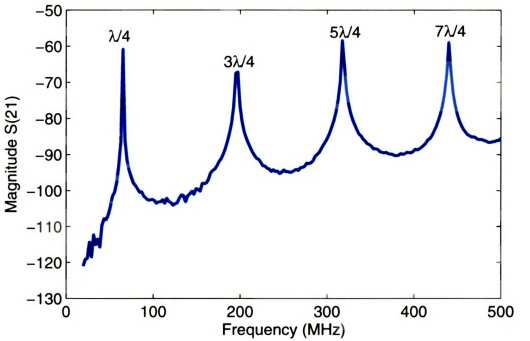


**Figure 19:** The first four resonant frequencies of the test setup of length 1.02 (m).

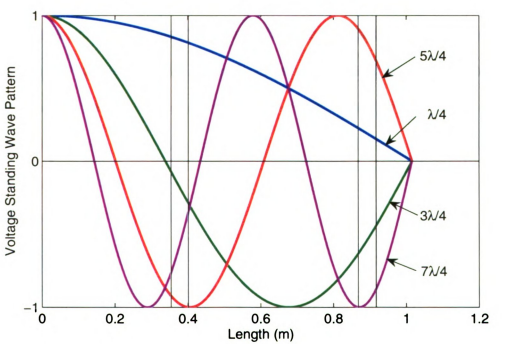


**Figure 20:** The voltage standing wave pattern for the resonant modes of the test setup.

To condition the FPC, the entire vacuum section of the coupler needs to be exposed to the full range of fields it will endure in actual cavity operation. By conditioning the FPCs any outgassing that is a result of ohmic heating will occur in the conditioning setup were the contaminants can be easily removed by the vacuum system without risking contamination to the accelerating cavity. Conditioning is also used to breakdown any multipacting barriers in the coupler. If the coupler was installed on the accelerating cavity and multipacting occurs, it could be difficult to distinguish whether it is the coupler or the cavity. Finally it is a much simpler to fix a bad coupler before installing it on a cavity.

The two-coupler test setup is able to condition the couplers by varying the short position to move the peak fields down the couplers. By varying the short position the resonant frequency of the setup is also varied. The peak voltage standing wave pattern is plotted in Figure 23 for the range of frequencies needed to condition the couplers; in this scenario the couplers must be switched to entirely condition them.

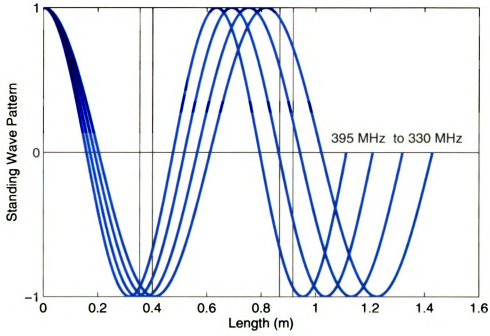


**Figure 21:** Voltage standing wave pattern for coupler conditioning spaning 330-395 MHz.

A standing wave method that can be used were the frequency is fixed is to construct the test setup with both ends as sliding shorts. By having both ends adjustable the frequency can be kept constant as the field patterns are varied. This method is favored for the reason that multipacting is a function of frequency so if the entire coupler is not conditioned at the operating frequency, multipacting barriers may have been skipped over.

## 4.5 Test Results

The two-coupler test setup was used to verify the power handling of the couplers. During testing soft multipacting barriers were encountered around 10 watts and up. The barriers were quickly and easily conditioned away by

sweeping the frequency and pulsing the generator at higher power levels. A power level of 1.27 kW was ultimately reached at 321 MHz where the design requires 1.01 kW. The power level at 321 MHz was limited by the generator power available.

The frequency of the test setup was then adjusted to 161 MHz where more generator power was available. A power level of 6.3 kW was reached by pulsing the generator power on and off. The limiting factor in the 161 MHz test was the inner conductor connection in the test setup. As the power level was increased, the inner conductor temperature increased, as expected due to rf losses in the conductor, causing the connecting sleeve to expand and loosen the rf connection. At first the loose connection appeared to be multipacting when only monitoring the line power of the test setup. When multipacting occurs, the vacuum pressure will change due to the electrons emitted into the vacuum. This was not the case since the vacuum pressure did not change. Another observation made was the suspect multipacting was dependent on the temperature of the inner conductor and not the power level. At this point it was easy to verify the loose connection by shaking the test setup which produced the same results as the suspected multipacting.

Figures 19 and 20 show the standing wave voltage approximation for two different tests were a line power of 1.27 kW at 321 MHz and 6.3 kW at 161 MHz was achieved. Based on the power levels achieved at 322 MHz and 161 MHz the coupler will be able to handle the lesser power required at 80.5 MHz without any issues.

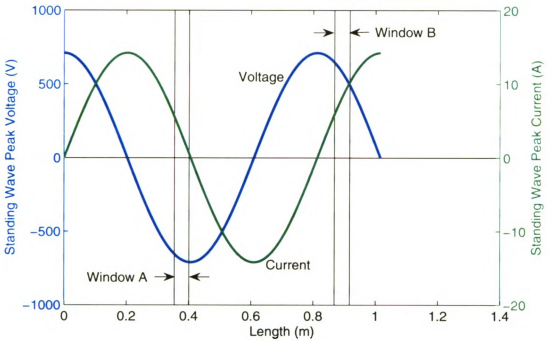


**Figure 22:** High power standing wave voltage and current pattern approximation for tests conducted at 321 MHz.

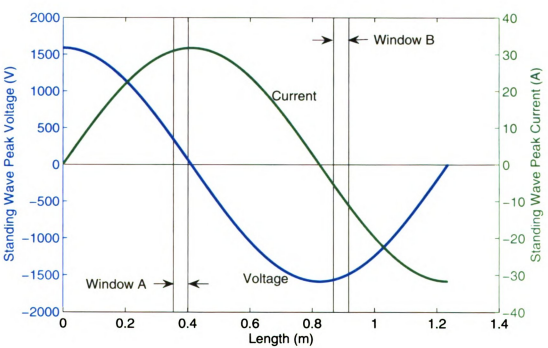


**Figure 23:** High power standing wave voltage and current pattern approximation for tests conducted at 161 MHz.

## CONCLUSION

The growing number of applications for superconducting accelerators has created a need for affordable accelerator designs. A low cost power coupler solution based on commercially available and affordable vacuum windows has been demonstrated for use with the Rare Isotope Accelerator $\beta = 0.085$ 80.5 MHz quarter-wave, and the $\beta = 0.285$ 322 MHz half-wave cavities. The FPC designs are able to achieve the coupling required to control the amplitude and phase of the beam. Two prototype FPCs have been tested to above the power levels required for their use in the RIA. The thermal and electrical properties of the FPCs have studied to create the best possible design with the best of both properties.

Construction of FPCs for the $\beta = 0.085$ 80.5 MHz quarter-wave and the $\beta = 0.285$ 322 MHz half-wave cavities are currently underway for use in a low beta test module. The module will be a functioning cryomodule containing the $\beta = 0.085$ 80.5 MHz quarter-wave and the $\beta = 0.285$ 322 MHz half-wave cavities along with the FPC designs that have been demonstrated. The couplers will then be tested in an actual module encompassing all the design goals of the low beta modules required for the RIA.

## APPENDIX

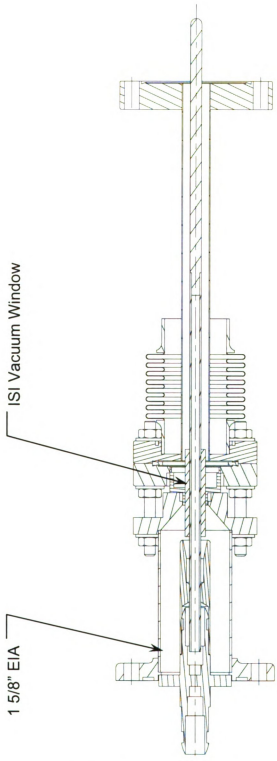


**Figure 24:** 322 MHz FPC cross section.

## APPENDIX

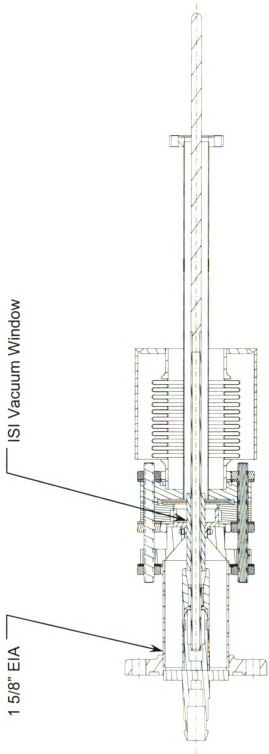


**Figure 25:** 80.5 MHz FPC cross section.

## REFERENCES


[1] National Superconducting Cyclotron Laboratory, "*The Rare Isotope Accelerator Conceptual Design Report*", NSCL, East Lansing, MI, to be published 2005.

[2] "*Completion of the LNL Bulk Niobium Low Beta Quarter Wave Resonators*", in Proceedings of the 9th Workshop on RF Superconductivity, Santa Fe, NM 1999.

[3] J. Bierwagen, S. Bricker, J. Colthorp, C. Compton, T. Grimm, W. Hartung, S. Hitchcock, F. Marti, L. Saxton, R. York, and A. Facco, "*Niobium Quarter-Wave Resonator Development for the Rare Isotope Accelerator*", in Proceedings of the 11th Workshop on RF Superconductivity, Travemunde, Germany, 2003.

[4] T. Grimm, J. Bierwagen, S. Bricker, W. Hartung, F. Marti, R. York, "*Experimental Study of a 322 MHz v/c=.28 Niobium Spoke Cavity*", in Proc. Of the 2003 IEEE Particle Accelerator Conference, Portland, OR, 2003.

[5] W. Hartung, C.C. Compton, T.L. Grimm, R.C. York, G. Ciovati, P. Kneisel, "*Status Report on Multi-cell Superconducting Cavity Development for Medium-velocity Beams*", in Proc. Of the 2003 IEEE Particle Accelerator Conference, Portland, OR, 2003.

[6] P. Kneisel, G. Ciovati, K. Davis, K. Macha and J. Mammosser, "*Superconducting Prototype Cavities for the Spallation Neutron Source*", in *8th European Particle Accelerator Conference*, Paris, 2002.

[7] H. Padamsee, J. Knoblock, T. Hays, "*RF Superconductivity For Accelerators*", John Wiley & Sons, Inc, 1998.

[8] J. Slater, "*Microwave Electronics*", D. Van Nostrand Company, Inc, 1950.

[9] J. Moore,C. Davis, M. Coplan, "*Building Scientific Apparatus 2nd*", Perseus Books Publishing, L.L.C., 1991.

[10] J. Lienhard IV, J. Lienhard V, "*A Heat Transfer Textbook 3rd*", Phlogiston Press, 2002.

[11] "*Cryogenics Technology Group Material Properties* ", National Instatute of Standards And Technology, http://cryogenics.nist.gov/NewFiles/material_properties.html

[12] D. Cheng, "*Field and Wave Electromagnetics*", Addison Wesley Publishing Company, Inc, 1992.

[13] R. Rabehl, "*Thermal Analysis of a Conductively Cooled Spallation Neutron Source (SNS) Fundamental Power Coupler*" FNAL, Batavia, IL, 2002.

[14] F. Incropera, D. DeWitt, "*Introduction To Heat Transfer*", Addison Wesley Publishing Company, Inc, 1992.

[15] Insulator Seal, Inc., "*High Vacuum Electrical And Optical Components*", Insulator Seal, Inc., Sarasota, FL, 1995.

[16] R. Harrington, "*Time-Harmonic Electromagnetic Fields*", IEEE Press, Wiley-Interscience, John Wiley & Sons, Inc, 2001.

[17] E. Somersalo, P. Yla-Oijala, D. Proch, "*Analysis of Multipacting in Coaxial Lines*," in Proceedings of the 1995 PAC, Dallas, TX, 1995.

## GENERAL REFERENCES

[18] Y. Kang, S. Kim, M. Doleans, I. Campisi, M. Stirbet, P. Kneisel, G. Ciovati, G. Wu, P. Yla-Oijala, "*Electromagnetic Simulations and Properties of the Fundamental Power Couplers for the SNS Superconducting Cavities*", in Proceedings of the 2001 Particle Accelerator Conference, Chicago, IL, 2001.

[19] T. Grimm, W. Hartung, M. Johnson, R. York, P. Kneisel, L. Turlington, "*Cryomodule Design for the Rare Isotope Accelerator*", in Proc. Of the 2003 IEEE Particle Accelerator Conference, Portland, OR, 2003.

[20] T. Grimm, W. Hartung, J. Popielarski, C. Compton, M. Johnson, Personal Communication, NSCL, East Lansing, MI.